Journal of Power Sources 196 (2011) 10791–10797

Contents lists available at SciVerse ScienceDirect

Journal of Power Sources

journal homepage: www.elsevier.com/locate/jpowsour

Electrochemical properties of leucoemeraldine, emeraldine, and pernigraniline forms of polyaniline/multi-wall carbon nanotube nanocomposites for supercapacitor applications

Seung-Beom Yoon, Eun-Hyea Yoon, Kwang-Bum Kim*

Department of Material Science and Engineering, Yonsei University, 134 Shinchon-Dong, Seodaemun-Gu, Seoul 120-749, Republic of Korea

ARTICLE INFO

Article history:
Received 18 July 2011
Received in revised form 25 August 2011
Accepted 26 August 2011
Available online 2 September 2011

Keywords:
Supercapacitor
Polyaniline
Multi-wall carbon nanotubes
Oxidation state
Specific capacitance

ABSTRACT

We report on the synthesis and electrochemical properties of leucoemeraldine base, emeraldine salt and pernigraniline base forms of polyaniline (PANI) in the form of nanocomposites with MWNTs. The oxidation state of PANI in the composite is controlled by doping and dedoping of the emeraldine salt form of PANI/MWNT composite, which is prepared through chemical polymerization, using oxidizing and reducing agents without changing the morphology of PANI in the composite and is confirmed by ultraviolet–visible spectroscopy (UV–vis) spectroscopy and Fourier transform infrared (FT-IR) spectroscopy. The electrochemical and pseudocapacitive properties of the composites are investigated using cyclic voltammetry and analyzed with respect to the oxidation state of polyaniline. The PANI/MWNT nanocomposites show specific capacitance values of 217 F g^{-1}, 328 F g^{-1} and 139 F g^{-1} for leucoemeraldine base, emeraldine salt and pernigraniline base, respectively. Electrochemical impedance spectroscopy is performed to explain the different electrochemical properties of PANI in different oxidation states.

1. Introduction

Polyaniline (PANI) has been investigated as one of the most promising candidates for electrodes in electrochemical capacitors (ECs) because of its easy synthesis, low cost, good environmental stability and relatively high specific capacitance [1–4]. Recently, there have been many studies on nanocomposites of PANI with carbon, especially multi-wall carbon nanotubes (MWNTs). MWNTs have a uniform diameter of several tens of nanometers, high surface area and high electrical conductivity, as well as unique properties such as a three-dimensional entangled structure on the nanometer scale [5–7]. These studies reported the improved electrochemical properties of PANI/MWNTs composites over PANI without MWNTs [8–10], because MWNTs create a porous structure with a highly accessible surface area and high electrical conductivity. However, there are wide variations in the specific capacitance of PANI/MWNT composites (from 177 F g^{-1} to 670 F g^{-1}) depending on the synthesis method, morphology and loading amount of PANI [11–16].

PANI exists in three redox forms with different oxidation states and can be interconverted between the fully reduced leucoemeraldine base (LB), the 50% intrinsically oxidized emeraldine base (EB), its doped emeraldine salt (ES), and the fully oxidized form of pernigraniline base (PB) [1]. PANI can store electrical energy through its redox transitions between the LB, ES, and PB forms [1,9]. The chemical, structural and electrical properties of PANI are known to be strongly dependent on its oxidation state [17,18].

Only a few studies have been reported on the pseudocapacitive properties of PANI with different oxidation states. Recently, Jamadade et al. reported the specific capacitance of the LB, ES, and PB forms of PANI that had been electrosynthesized on a stainless steel substrate. However, each form of PANI had a different deposit morphology and showed cyclic voltammograms that are not typical of PANI and are severely distorted with potential scan rate [11].

In this study, we report the pseudocapacitive properties of the LB, ES, and PB forms of PANI in the form of nanocomposites with MWNTs. The oxidation state of PANI in the composites was controlled by doping and de-doping of the ES form of PANI/MWNT composite, which was prepared through chemical polymerization, using oxidizing and reducing agents without changing the morphology of the PANI in the composite. The morphological and structural properties of PANI in the composites were investigated using SEM, TEM, FT-IR and UV–vis spectroscopy. The electrochemical characteristics of the composites were evaluated in order to investigate the pseudocapacitive properties of PANI with different oxidation states by using the cyclic voltammetry. Electrochemical impedance spectroscopy (EIS) was performed using a cavity-microelectrode (CME) in order to explain the different electrochemical properties of the LB, ES, and PB forms of PANI.

* Corresponding author. Tel.: +82 2 365 7745; fax: +82 2 312 5375.
E-mail address: kbkim@yonsei.ac.kr (K.-B. Kim).

0378-7753/$ – see front matter © 2011 Elsevier B.V. All rights reserved.
doi:10.1016/j.jpowsour.2011.08.107

2. Experimental details

2.1. Materials

For the preparation of the PANI/MWNT composites, commercial MWNTs (ILJIN Nanotech Co., Ltd. South Korea) were used. The MWNTs have diameters of 10–20 nm, lengths of 10–50 μm and a BET surface area of 200 $m^2\ g^{-1}$. To introduce hydrophilic functional groups onto their surface, the MWNTs were treated with nitric acid (Duksan Chem., 98%) in a glass beaker at 80 °C for 4 h. The treated MWNTs were then rinsed with distilled water several times, filtered and then dried in an oven overnight.

Aniline, ammonium persulfate (APS), phenyl hydrazine, and HCl were purchased from Sigma–Aldrich. Aniline monomer was purified at a temperature over the boiling point of aniline by distillation to remove any impurities and oligomers. APS was used as the oxidizing agent for polymerization. Phenyl hydrazine was selected as the reducing agent.

2.2. Preparation of PANI/MWNT composites with different chemical states

The ES/MWNT composite was prepared as follows. The acid-treated MWNTs (60 mg) were dispersed in 80 mL of 1 M HCl solution by ultrasonication and the distilled aniline monomer (240 mg) was added to the MWNT suspension in 1 M HCl solution. APS dissolved in 20 mL of 1 M HCl solution was added to the suspension dropwise with constant mechanical stirring (the molar ratio of APS/aniline was 2.3). After 24 h, the ES/MWNT composite was synthesized *via in situ* chemical oxidation polymerization. The resulting green suspension was filtered and the residue was washed with methanol and distilled water repeatedly. The ES/MWNT composite powder was dried by vacuum–freeze–drying for 48 h. The oxidation state of PANI in the composite was controlled by chemical oxidation and reduction of the ES form of PANI/MWNT composite using oxidizing and reducing agents in order to minimize the morphological change of the PANI in the composite.

The fully reduced LB/MWNT composite was prepared from the ES/MWNT powder by chemical reduction using phenyl hydrazine. The ES/MWNT powder was immersed in a solution of phenyl hydrazine with mechanical stirring until the powder color changed from the green color of ES/MWNT to the colorless or light yellow color of LB/MWNT corresponding to the fully reduced and de-doped state of PANI. After the reaction was complete, the LB/MWNT composite was filtered and washed exhaustively with methanol and distilled water repeatedly to completely remove the phenyl hydrazine. The LB/MWNT powder was dried by vacuum–freeze–drying for 48 h.

The fully oxidized PB/MWNT composite was prepared by chemical oxidation using APS solution. The ES/MWNT powder was immersed in APS solution until it changed from the green color of ES/MWNT to the violet color of PB/MWNT. In this synthetic process, the ES/MWNT powder was excessively oxidized. After the chemical oxidation reaction, the PB/MWNT composite was filtered and washed exhaustively with methanol and distilled water repeatedly, and then dried by vacuum–freeze–drying for 48 h.

The oxidation state of the LB, ES, and PB forms of PANI in the composite was investigated using ultraviolet–visible spectroscopy (UV–vis) and Fourier transform infrared (FT-IR) spectroscopy.

2.3. Characterization

The morphology of the PANI/MWNT composite was examined using field-emission scanning electron microscopy (FE-SEM, S-4300SE, HITACHI) and field-emission transmission electron microscopy (FE-TEM, JEM-2100F, JEOL). UV–vis spectra were recorded on a Perkin Elmer Lambda 900 with the composites dispersed in NMP solution. FT-IR spectra were recorded between 4000–450 cm^{-1} at a spectral resolution of 4 cm^{-1} on a Perkin Elmer 1710 spectrophotometer using potassium bromide (KBr) pellets at room temperature.

2.4. Electrochemical measurements

For the electrochemical measurements, PANI/MWNT composite electrodes were fabricated using the following process. The electrodes were fabricated by slurry casting of 80 wt.% active material (PANI/MWNT composites), 15 wt.% acetylene black, and 5 wt.% polyvinylidene fluoride (PVDF) binder dissolved in *N*-methylpyrrolidone (NMP) solvent. The electrode was prepared on titanium foil as the current collector. The exposed nominal area was 1 cm × 1 cm. The weight of the PANI/MWNT composite on the titanium foil current collector in this study was *ca.* 1 mg cm^{-1}.

Electrochemical measurements were performed in a three-electrode electrochemical cell where the PANI/MWNT composite electrode was used as the working electrode; a platinum plate and a saturated calomel electrode (SCE) were used as the counter and reference electrodes, respectively. Cyclic voltammetry (CV) was performed using a potentiostat/galvanostat (Solartron 1470E, Cell Test System) in 1 M H_2SO_4 aqueous solution in the potential window from −0.2 to 0.8 V_{SCE}. The current response in the CV curves was normalized with respect to the mass of the PANI/MWNT composites. Electrochemical impedance spectroscopy (EIS) measurements for the composites were performed under 0.25 V_{SCE} in the AC frequency range from 200 000 to 0.01 Hz and ac amplitude of 5 mV using an impedance analyzer (Solartron, 1260A Impedance/Gain-Phase Analyzer).

3. Results and discussion

3.1. Morphology of the PANI/MWNT composites

Scanning electron microscopy (SEM) and transmission electron microscopy (TEM) were used to investigate the morphology of the PANI/MWNT composites. Fig. 1(a)–(c) shows SEM images of the PANI/MWNT composites for the LB, ES and PB forms of PANI, respectively. It can be clearly seen that PANI was selectively deposited only on the surface of the MWNTs without blocking the pores in their entangled structure. Since the LB and PB forms of PANI in the composites were derived from the ES form of PANI by chemical reduction and oxidation, respectively, they all have similar morphologies. The TEM images of the PANI/MWNT composites for the LB, ES and PB forms of PANI in Fig. 1(d)–(f) show average thicknesses of 20 nm of PANI coated on the surface of the MWNTs. If we assume that all of the aniline monomer was polymerized onto the MWNTs, the loading amount of PANI in the composite would be 80 wt.%.

3.2. Oxidation states of the PANI/MWNT composites

UV–vis spectroscopy was used to examine the oxidation states of PANI in the composites. The UV–vis spectra of the acid-treated MWNTs in Fig. 2(a) do not exhibit any absorption peaks. In contrast, Fig. 2(b)–(d) shows that the LB/MWNT, ES/MWNT and PB/MWNT composites exhibit intrinsic absorption peaks. The presence of three peaks at around 345, 415 and 800 nm in the spectrum of ES/MWNT in Fig. 2(c) confirms the existence of the conducting ES form [19]. The peak at 345 nm is attributed to a π–π^* transition of the bezenoid moiety, the peak at 415 nm to the polaron–π^* transition, and the peak at 800 nm to the π–polaron transition [19]. The absorption peak at about 320 nm for the LB/MWNT composite in Fig. 2(b) is attributed to a π–π^* transition of the bezenoid moiety

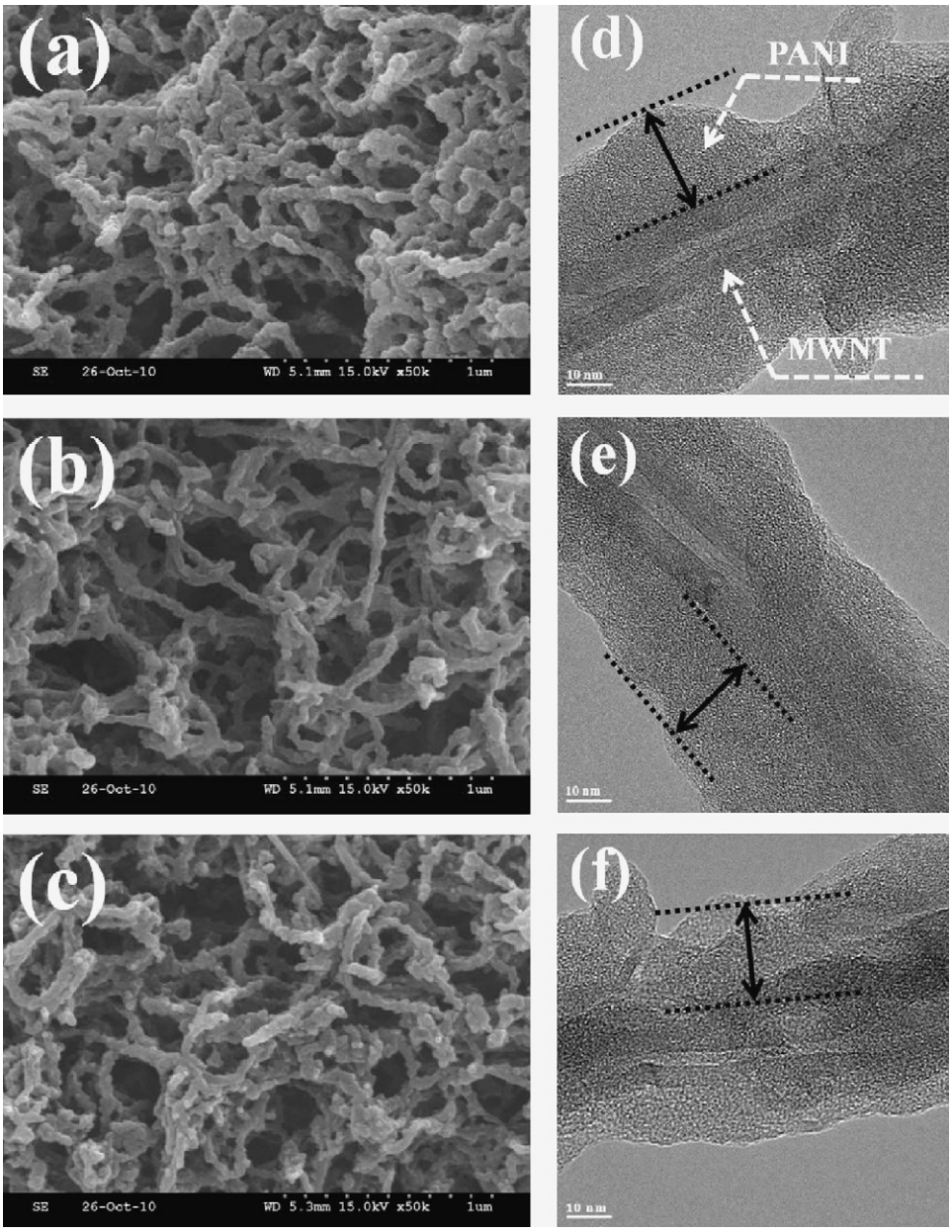

Fig. 1. SEM images of (a) LB/MWNT, (b) ES/WMNT and (c) PB/MWNT composites, and TEM images of (d) LB/MWNT, (e) ES/MWNT and (f) PB/MWNT composites.

in the molecule [20]. The UV–vis spectra in Fig. 2(b) indicate that the LB/MWNT composite contains an insulating form of LB, in the fully reduced state, and that the phenyl hydrazine solution was completely removed from it [22]. The 550 nm peak of the PB/MWNT composite in Fig. 2(d), which is ascribed to a Peierls gap transition in pernigraniline, reflects the fully oxidized state of PANI [21,22].

Fig. 3(a)–(d) shows the FT-IR spectra of the acid-treated MWNTs and LB/MWNT, ES/MWNT and PB/MWNT composites recorded in the range of 2000 to 1200 cm^{-1} at ambient temperature, respectively. All of the spectra have three bands at 1580 cm^{-1}, 1495 cm^{-1} and 1300 cm^{-1} which are attributed to quinoid-ring stretching, benzene-ring stretching and C–N stretching, respectively [23]. In the case of the acid-treated MWNTs, the weak C–N stretching peak in Fig. 3(a) is due to their acid treatment with nitric acid [24]. Fig. 3(b)–(d) shows that the C–N stretching peak of the acid-treated MWNTs at 1300 cm^{-1} is greatly enhanced by its superposition with the C–N stretching peak of PANI present at approximately the same frequency [23]. Furthermore, the LB/MWNT, ES/MWNT and PB/MWNT composites exhibit the characteristic bands of PANI at about 1580 and 1495 cm^{-1} [25]. Since these bands are due to the quinoid-ring stretching and benzene-ring stretching, respectively, their intensity ratio (I_{1580}/I_{1495}) could be used as an indicator of the degree of oxidation of PANI [25,26]. Fig. 3(b) and (c) shows that the I_{1580}/I_{1495} intensity ratio of LB/MWNT is lower than those of ES/MWNT and PB/MWNT, due to the predominating presence of benzene-ring units in LB/MWNT. The I_{1580}/I_{1495} intensity ratio of ES/MWNT is smaller than that of PB/MWNT; this indicates that the oxidation level of PANI in the composite increases in the order LB/MWNT < ES/MWNT < PB/MWNT. A similar result was reported by Choi et al. [25]. The slightly higher intensity of the quinoid-ring stretching peak compared to that of the benzene-ring stretching peak in PB/MWNT might be due to the quinoid-ring introduced during the acid-treatment of the MWNTs.

The analysis of the UV–vis spectra and FT-IR spectra of the acid-treated MWNTs and LB/MWNT, ES/MWNT and PB/MWNT composites indicates that PANI was selectively deposited on the

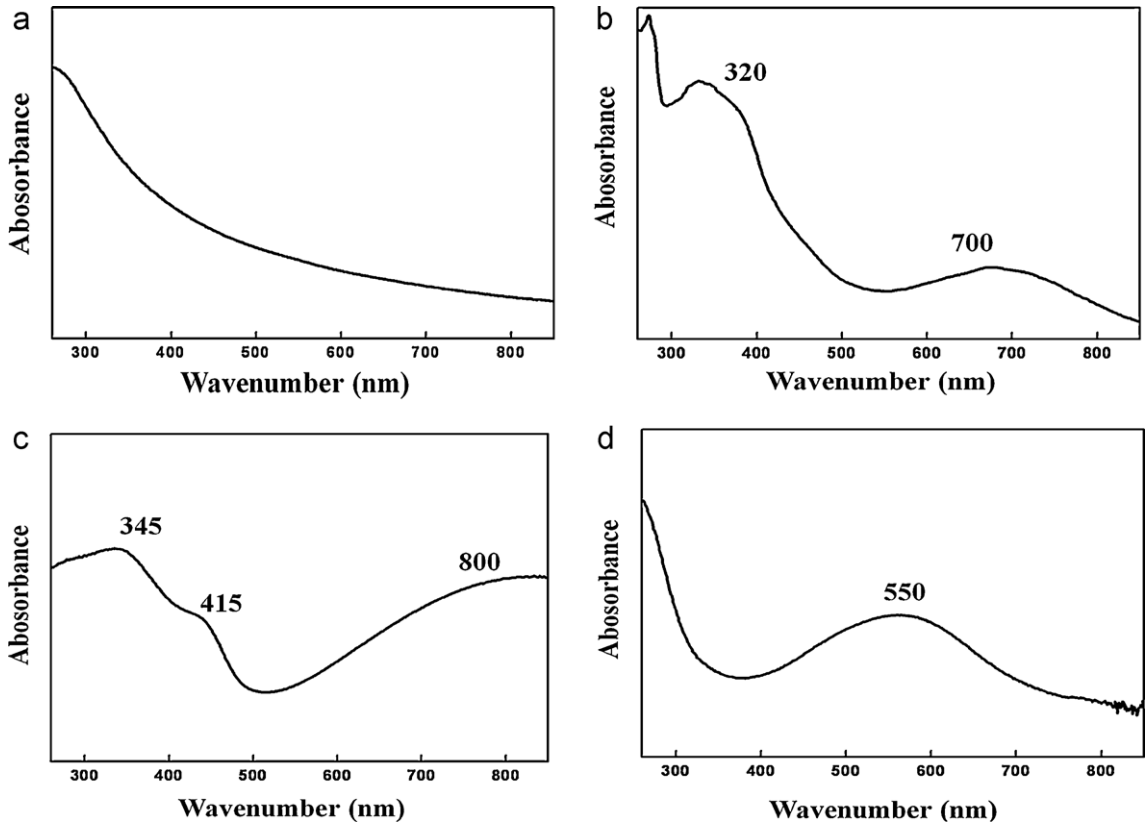

Fig. 2. UV–vis spectra of (a) acid treated MWNTs and (b) LB/MWNT, (c) ES/MWNT and (d) PB/MWNT composites.

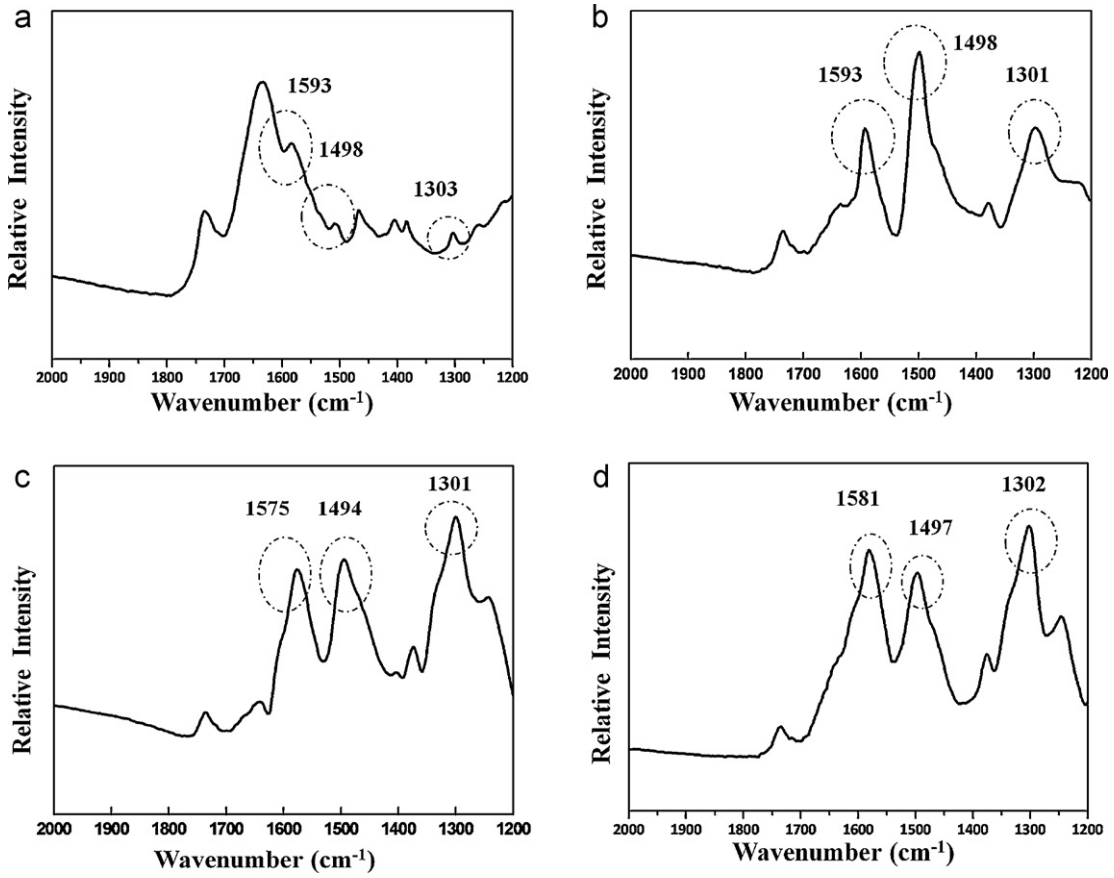

Fig. 3. FT-IR spectra of 2000–1200 cm^{-1} region of (a) acid treated MWNTs and (b) LB/MWNT, (c) ES/MWNT and (d) PB/MWNT composites.

surface of the MWNTs to form a nanocomposite of PANI with the MWNTs by chemical polymerization and that the oxidation state of PANI could be successfully controlled from ES/MWNT to LB/MWNT or PB/MWNT by using oxidizing and reducing agents, respectively.

3.3. Electrochemical properties of PANI/MWNT composites

3.3.1. Cyclic voltammetry measurements

CV was used to investigate the electrochemical properties of the LB/MWNT, ES/MWNT and PB/MWNT composites window of −0.2 to 0.8 V (vs SCE) at scan rates of 5, 10, 30, and 50 mV s^{-1} in 1 M H_2SO_4 solution. Fig. 4(a)–(c) illustrates the CV curves of these three forms of PANI/MWNT composites at a scan rate of 5 mV s^{-1}, respectively. PANI in the composite has a unique cyclic voltammogram depending on its oxidation state. It is clear that PANI has three pairs of redox peaks (A_1/C_1, A_2/C_2 and A_3/C_3) [27–30]. Peaks A_1/C_1 correspond to the redox transition of PANI between LB and ES, peaks A_2/C_2 represent the by-products and intermediates of the hydroquinone/benzoquinone redox reaction, and peaks A_3/C_3 are attributed to the redox transition of PANI between ES and PB [27–30]. During the cyclic voltammetry of PANI, PANI may take the ES, LB or PB form depending on its electrode potential, i.e. its oxidation state. Therefore, it may be speculated that the LB, ES, and PB forms of PANI should have the same electrochemical behavior. However, the LB, ES, and PB forms of PANI showed different cyclic voltammograms in this study. As shown in Fig. 4(a), the cyclic voltammograms become severely distorted and the peak potential separation of the redox couples increases with increasing potential scan rate. The overall shape of the cyclic voltammograms of ES/MWNT in Fig. 4(b) is well maintained and the peak potential separation of the redox couples increases slightly with increasing potential scan rate. This reflects the high electrochemical reversibility of ES in the composite. Furthermore, ES/MWNT exhibits the highest normalized current response with respect to the mass of the composite among the three different PANI composites with different oxidation states. Fig. 4(c) shows that the cyclic voltammograms of PB/MWNT are well maintained and that the peak potential separation of the redox couples increases very slightly with increasing potential scan rate, however, PB/MWNT exhibits the lowest normalized current response.

The specific capacitances of the PANI/MWNT composites were calculated from the following equation:

$$C_s = \frac{\int 1_a dt + \left| \int 1_c dt \right|}{2M\Delta V} \quad (1)$$

where C_s, I_a, I_c and ΔV indicate the specific capacitance, anodic current, cathodic current and potential range, respectively. M is the mass of the composite. The plots of the specific capacitance of the PANI/MWNT composites as a function of the potential scan rate are shown in Fig. 5(a). The specific capacitances were calculated to be 217 F g^{-1}, 328 F g^{-1} and 139 F g^{-1} of the composite for LB/MWNT, ES/MWNT and PB/MWNT, respectively, at 5 mV s^{-1}. ES/MWNT shows the highest specific capacitance and PB/MWNT the lowest.

Fig. 5(b) shows the normalized capacitances of the LB/MWNT, ES/MWNT and PB/MWNT nanocomposites as a function of the potential scan rate. The normalized capacitance at each scan rate was obtained by dividing the specific capacitance by the specific capacitance measured at 5 mV s^{-1}. As shown in Fig. 5(b), LB/MWNT and ES/MWNT showed similar capacitance losses of 21% and 23%, respectively, in the range of scan rates from 5 to 50 mV s^{-1}. The PB/MWNT composite, which has the lowest specific capacitance, showed the highest rate capability.

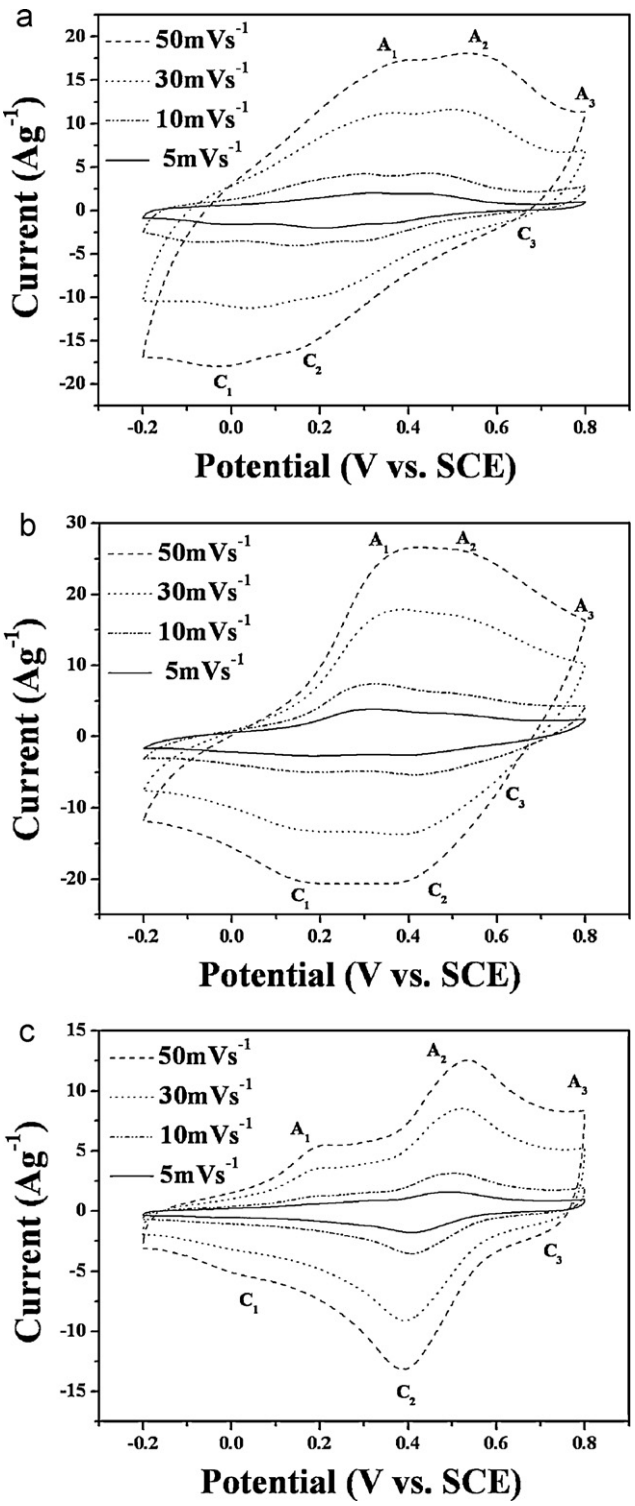

Fig. 4. CV curves of (a) LB/MWNTs, (b) ES/MWNT and (c) PB/MWNT composites at different scan rates in 1 M H_2SO_4.

3.3.2. Electrochemical impedance spectroscopy measurements

EIS was performed in order to explain the different electrochemical properties of the LB, ES, and PB forms of PANI in the composite. In this study, the impedance measurements of the composites were made using a cavity-microelectrode (CME). A CME is an efficient tool to investigate the electrochemical kinetics of processes occurring at a powder material electrode. Because only a small amount of

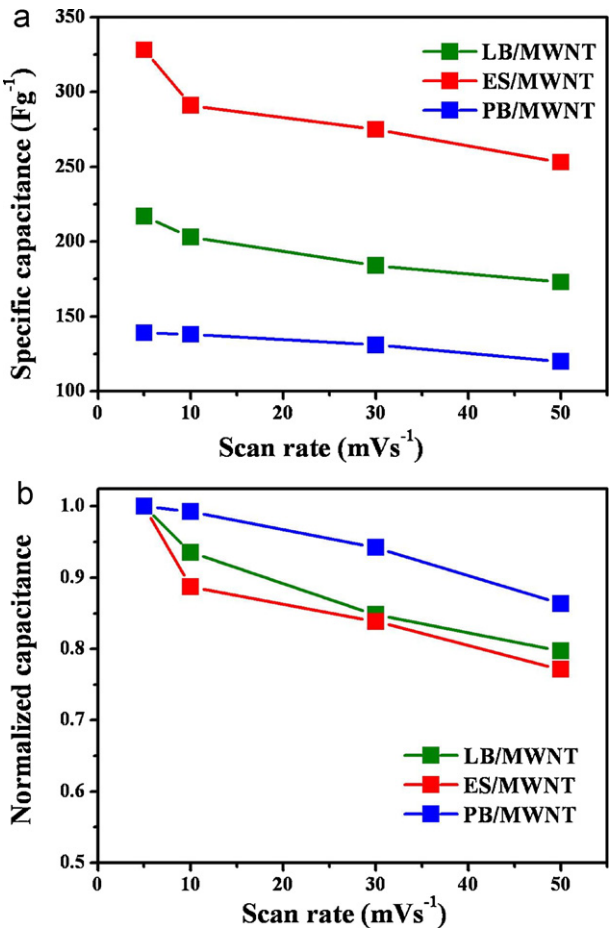

Fig. 5. Specific capacitance (a) and normalized capacitance (b) of LB/MWNT, ES/MWNT and PB/MWNT composites as a function of potential scan rate.

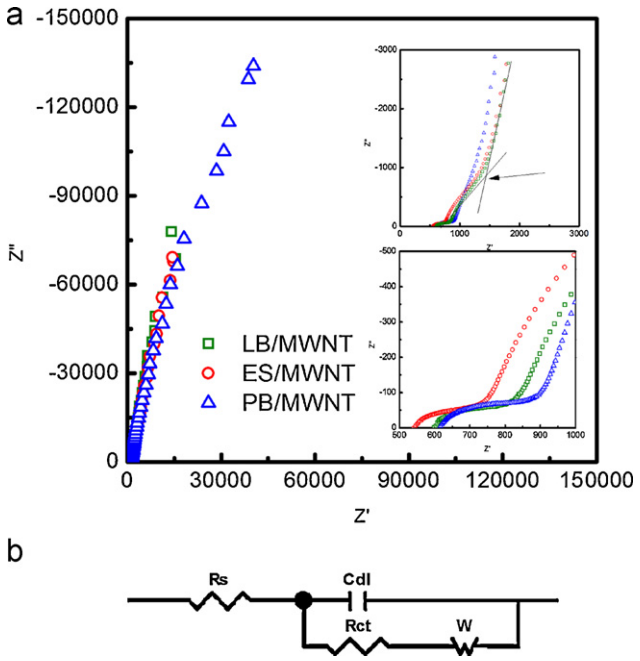

Fig. 6. (a) Nyquist plots of PANI/MWNT composites measured at different oxidation states and (b) equivalent circuit model for the EIS analysis.

powder (hundreds of micrograms) is characterized, the ohmic drop arising from the bulk of the electrolyte can be neglected [31–33].

Fig. 6(a) shows the Nyquist plot of the LB/MWNT, ES/MWNT and PB/MWNT composites, which is composed of a semi-circle in the high frequency region and an inclined line in the low frequency region. The equivalent circuit model for the Nyquist plot in Fig. 6(b) is comprised of series resistance (R_s), electrical double layer capacitance (C_{dl}), charge-transfer resistance (R_{ct}) and Warburg impedance (W). A semi-circle in the high frequency region corresponds to R_s, C_{dl} and R_{ct}. An inclined line in the low frequency region is related to W. In this study, the PB/MWNT composite differs from the other composites in that the inclined line for the PB/MWNT composite shows a single nearly vertical line, while the LB/MWNT and ES/MWNT composites have an inclined line composed of two lines that have different slopes, the 45° line and nearly vertical line (upper inset, Fig. 6). The inclined line at low frequency is usually attributed to a porous structure electrode [34] or the penetration of the electroactive species into the active materials [35]. Since there is little difference in the deposit morphology and thickness of PANI in the composites, the inclined line could be attributed to the diffusion limitation of ions in the active materials, which is often referred to as the Warburg impedance. The 45° line in the Warburg impedance is related to ion (SO_4^-) diffusion in the PANI layer on the MWNTs. The vertical line at lower frequencies parallel to the imaginary axis indicates a capacitive behavior and represents the accumulation of diffused ions in the structure. In the case of the PB/MWNT, the 45° line is absent and the nearly vertical line is observed after the semi-circle in the Nyquist plot. The absence of the 45° line and the lowest specific capacitance of the PB/MWNT composite suggest that electrochemical reaction is limited to the surface layer of PANI in the PB/MWNT composite.

A semi-circle at high frequency can be seen more clearly in the lower inset of Fig. 6. The point intersecting with the real axis indicates R_s, which is composed of the solution resistance, contact resistance and intrinsic resistance of the active material. The diameter of the semi-circle is the R_{ct}. The ES/MWNT composite has smaller R_s and R_{ct} than the LB/MWNT and PB/MWNT composites because of the high electrical conductivity of the ES form of PANI in the composite. Higher specific capacitance of the ES/MWNT composite could be attributed to the smaller values of R_s and R_{ct}.

4. Conclusions

Nanocomposites of leucoemeraldine base, emeraldine salt and pernigraniline base with MWNTs are successfully prepared through the chemical polymerization of ES/MWNT followed by control of its oxidation state by using oxidizing and reducing agents, respectively. SEM and TEM analysis shows that PANI is selectively deposited only on the surface of the MWNTs without blocking the pores in their entangled structure. The morphology of the PANI in the composite is maintained after chemical oxidation and reduction treatment. The average thickness of the PANI coated on the surface of the MWNTs is about 20 nm, and the loading amount of PANI in the composite is 80 wt%. The analysis of the UV–vis spectra and FT-IR spectra of the acid-treated MWNTs and composites confirmed that PANI is selectively deposited on the surface of the MWNTs to form a nanocomposite of PANI with the MWNTs and that the oxidation state of PANI can be successfully controlled from the emeraldine salt to the leucoemeraldine base or the pernigraniline base by using oxidizing and reducing agents, respectively. The electrochemical and pseudocapacitive properties of the composites are investigated using cyclic voltammetry and analyzed with respect to the oxidation state of PANI. PANI in the composite has unique CV depending on its oxidation state and each cyclic voltammogram shows capacitive-like responses with three pairs of redox peaks in the whole potential range of investigation. PANI/MWNT nanocomposites show specific capacitances of 217 F g^{-1}, 328 F g^{-1}

and 139 F g^{-1} at 5 mV s^{-1} for the leucoemeraldine base, the emeraldine salt and the pernigraniline base, respectively. Electrochemical impedance spectroscopy is performed to explain the different electrochemical properties of PANI with different oxidation states.

Acknowledgements

This work was supported by the National Research Laboratory Program through the National Research Foundation of Korea (NRF) grant funded by the Ministry of Education, Science and Technology (MEST) (Grant No.: 2007-0055835) and by a Manpower Development Program for Energy & Resources supported by the Ministry of Knowledge and Economy (MKE).

References

[1] E.T. Kang, K.G. Neoh, K.L. Tan, Prog. Polym. Sci. 23 (1998) 227–324.
[2] Y.K. Zhou, B.L. He, W.J. Zhou, Electrochim. Acta 49 (2004) 257–262.
[3] Y.K. Zhou, B.L. He, W.J. Zhou, H.L. Li, J. Electrochem. Soc. 151 (2004) A1052–A1057.
[4] K.R. Prasad, N. Munichand, J. Power Sources 112 (2002) 443–451.
[5] J.H. Park, J.M. Ko, O.O. Park, J. Electrochem. Soc. 150 (2003) A864–A867.
[6] J.H. Kim, K.W. Nam, K.B. Kim, Korean Patent 2004/10–2004–0099039 (2004).
[7] J.H. Kim, K.B. Kim, Carbon 44 (2006) 1963–1968.
[8] E. Frackowiak, Phys. Chem. Chem. Phys. 9 (2007) 1774–1785.
[9] V. Mottaghitalab, B. Xi, G.M. Spinks, G.G. Wallace, Synth. Met. 156 (2006) 796–803.
[10] T. Wu, S. Lin, J. Polym. Sci. B: Polym. Phys. 44 (2006) 1413–1418.
[11] V.S. Jamadade, D.S. Dhawale, C.D. Lokhande, Synth. Met. 160 (2010) 955–960.
[12] Y. Zhou, Z.Y. Qin, L. Li, Y. Zhang, Y.L. Wei, Electrochim. Acta 55 (2010) 3904–3908.
[13] L. Li, Z.Y. Qin, X. Liang, Q.Q. Fan, J. Phys. Chem. C 113 (2009) 5502–5507.
[14] H. Li, J. Wang, Q. Chu, Z. Wang, F. Zhang, J. Power Sources 190 (2009) 578–586.
[15] V. Gupta, N. Miura, Electrochim. Acta 52 (2006) 1721–1726.
[16] J. Zhang, L.B. Kong, B. Wang, Y.C. Luo, Synth. Met. 159 (2009) 260–266.
[17] W.S. Huang, B.D. Humphrey, A.G. MacDiarmid, J. Chem. Soc. Faraday Trans. 82 (1986) 2385–2400.
[18] S. Quillard, K. Berrada, G. Louarn, S. Lefrant, M. Lapkowski, A. Pron, New J. Chem. 19 (1995) 365–370.
[19] L. Pan, L. Pu, Y. Shi, T. Sun, R. Zhang, Y. Zheng, Adv. Funct. Mater. 16 (2006) 1279–1288.
[20] M.K. Ram, G. Mascetti, S. Paddeu, E. Maccioni, C. Micolini, Synth. Met. 89 (1997) 63–69.
[21] N. Gospodinova, L. Terlemezyan, P. Mokreva, K. Kossev, Polymer 34 (1993) 2434–2437.
[22] J.E. Albuquerque, L.H.C. Mattoso, Synth. Met. 113 (2000) 19–22.
[23] S. Tan, D. Belanger, J. Phys. Chem. B 109 (2005) 23480–23490.
[24] K. Jiang, A. Eitan, L.S. Schadler, P.M. Ajayan, Nano Lett. 3 (2003) 257–261.
[25] B.G. Choi, H.S. Park, H.S. Im, Y.J. Kim, J. Membr. Sci. 324 (2008) 102–107.
[26] M. Ludvigsson, J. Lindgren, Electrochim. Acta 45 (2000) 2267–2271.
[27] T. Kobayashi, H. Yoneyama, H. Tamura, J. Eelectroanal. Chem. 177 (1984) 293–298.
[28] E.M. Genies, C. Tsintavis, J. Eelectroanal. Chem. 195 (1985) 109–112.
[29] A. Kitani, M. Kaya, J. Yano, K. Yoshikawa, K. Sasaki, Synth. Met. 18 (1987) 341–347.
[30] R.M. Karim, C.J. Lee, Y.T. Park, M.S. Lee, Synth. Met. 151 (2005) 131–135.
[31] C. Cachet-Vivier, V. Vivier, C.S. Cha, J.-Y. Nedelec, L.T. Yu, Electrochim. Acta 47 (2001) 181–189.
[32] C. Portet, J. Chmiola, Y. Gogotsi, S. Park, K. Lyan, Electrochim. Acta 53 (2008) 7675–7680.
[33] R. Lin, P.L. Taberna, J. Chmiola, D. Guay, Y. Gogotsi, P. Simon, J. Electrochem. Soc. 156 (2009) A7–A12.
[34] S. Zhang, C. Peng, K.C. Ng, G.Z. Chen, Electrochim. Acta 55 (2010) 7447–7453.
[35] A.J. Roberts, R.C.T. Slade, Electrochim. Acta 55 (2010) 7460–7469.